



Originally published as:

Rabizadeh, T., Morgan, D. J., Peacock, C. L., Benning, L. G. (2019): Effectiveness of Green Additives vs Poly(acrylic acid) in Inhibiting Calcium Sulfate Dihydrate Crystallization. - *Industrial and Engineering Chemistry Research*, 58, 4, pp. 1561—1569.

DOI: <http://doi.org/10.1021/acs.iecr.8b02904>

# Effectiveness of green additives *vs.* poly(acrylic acid) in inhibiting calcium sulfate dihydrate crystallization

Taher Rabizadeh<sup>1,2\*</sup>, David J. Morgan<sup>3</sup>, Caroline L. Peacock<sup>1</sup>, Liane G. Benning<sup>1,4,5\*</sup>

1- School of Earth and Environment, University of Leeds, Leeds, LS2 9JT, United Kingdom

2- Department of Materials Engineering, Faculty of Mechanical Engineering, University of Tabriz, 51666-16471, Tabriz, Iran

3- Cardiff Catalysis Institute, School of Chemistry, Cardiff University, Cardiff, CF10 3AT, United Kingdom

4- GFZ, German Research Centre for Geosciences, Telegrafenberg, 14473 Potsdam, Germany

5- Department of Earth Sciences, Free University of Berlin, 12249 Berlin, Germany

\* Correspondence to: Taher Rabizadeh (t.rabizadeh@tabrizu.ac.ir) and Liane G. Benning (Benning@gfz-potsdam.de)

**Keywords:** crystallization, calcium sulfate dihydrate, antiscalant, surface adsorption, poly(acrylic acid), X-ray photoelectron spectroscopy

**Abstract:** The effects that 20 ppm poly(epoxysuccinic acid) (PESA), poly(aspartic acid) (PASP) and two poly(acrylic acid) (PAA) compounds with molecular weights of ~ 2000 and ~100000, have on the crystallization of gypsum were evaluated at 21 °C by *in situ* UV-Vis spectrophotometry. XRD and SEM were utilized for phase and morphological studies, while the way these additives are associated with the final gypsum crystals was evaluated by XPS. The comparison showed that PASP performed far better than the other antiscalants as it

completely inhibited the formation of gypsum. In contrary, the presence of the low molecular weight PAA decreased the rate of crystallization far more than the larger molecular weight PAA. When the pH in the reacting solution was switched from  $\sim 4$  to  $\sim 7$ , the efficiency of the low molecular weight PAA in inhibiting gypsum formation increased, while in the presence of the higher molecular weight PAA the opposite effect was observed.

## 1. Introduction

In many industrial processes that rely on water handling systems (e.g., oil and gas production, water desalination, water treatment, cooling systems, etc.), the formation of mineral scales in pipes, filters and heat exchangers has detrimental consequences to process efficiency.<sup>1</sup> These include flow reduction, notable depression in the heat transfer efficiency and clogging of pipes, valves and other equipment, as well as other side effects such as corrosion which all result in efficiency losses.<sup>2,3</sup> Common scale deposits are calcium carbonate,<sup>4</sup> silica,<sup>5</sup> barium sulfate,<sup>6</sup> and calcium sulfate<sup>7</sup> known as sparingly soluble crystals. In a large number of water handling processes, calcium sulfate scales form preferentially and they are more stable than other scale types because their formation is pH independent (i.e., they can precipitate at pH as low as 2)<sup>8</sup> and this leads to serious problems in many industrial water processing activities.<sup>9</sup> Cleaning or removing mineral scales is costly and they affect the efficiency and lifetime of processing technologies.<sup>10</sup> It is, therefore, preferable to prevent scale formation rather than remove scale products. In the calcium sulfate system, three phases with various degrees of hydration exist: the dihydrate gypsum ( $\text{CaSO}_4 \cdot 2\text{H}_2\text{O}$ ), the hemihydrate bassanite ( $\text{CaSO}_4 \cdot 0.5\text{H}_2\text{O}$ ), and the anhydrous anhydrite ( $\text{CaSO}_4$ ).<sup>11</sup> As with many other sparingly soluble salts, temperature, supersaturation and the presence of impurities, affect the formation and solubility of the different polymorphs.<sup>12</sup>

Various methods to inhibit, reduce or prevent the formation of calcium sulfate scales have been proposed. Among them, the addition of inhibitors or antiscalants is the most economical and is more efficient than acid washing or mechanical cleaning.<sup>13,14</sup> Antiscalants are generally divided into nonpolymeric (e.g., hexametaphosphates, phosphonates)<sup>15</sup> and polymeric (e.g., polycarboxylates)<sup>16</sup>, and their application and effects on mineral scaling have been extensively studied.<sup>2</sup> It has been suggested that antiscalants can prevent scale formation by different ways, such as through sequestration or chelation of the ions in solution that are required for mineral precipitation, increasing the interfacial tension between nuclei and the solution, dispersing scale mineral crystallites, and / or adsorbing to the growing scale mineral surfaces.<sup>4</sup> However, a molecular level understanding of the mechanisms by which antiscalants prevent mineral scaling is still lacking.

In addition, the post-reaction disposal of such industrial inhibitors leads to pollution of the environment.<sup>17-19</sup> For example, when such P and N containing compounds reach water ways, they play a key role in eutrophication which can cause major ecological damage.<sup>19</sup> Therefore, the concept of “Green Chemistry” was proposed and scale inhibitors that are not detrimental to our environment have become a recent focus for inhibiting industrial scale formation.<sup>20,21</sup>

Among green inhibitors, poly(epoxysuccinic acid) (PESA) and poly(aspartic acid) (PASP) are the most common and promising environmentally friendly polycarboxylate antiscalants. They are both highly biodegradable and non-toxic,<sup>22</sup> two of the main criteria of a “green” inhibitor. PESA and PASP have both been extensively used in various industrial applications such as water treatment.<sup>23</sup> However, to date, studies that evaluate the effects of different poly(carboxylic acid) inhibitors on gypsum precipitation have primarily focused on changes in precipitation onset, or the effect of high temperatures.<sup>24-27</sup> Therefore, a mechanistic understanding of the effects that different poly(carboxylic acids), particularly the

green ones, have on gypsum formation is still lacking. How these inhibitors operate, and how they can be optimized to inhibit scale formation, are poorly understood. Indeed, in some cases, it is still unclear whether the commonly used conventional less-biodegradable polycarboxylic inhibitors (e.g., polyacrylic acid) can be replaced by greener equivalents (e.g., PESA and PASP).

To address these gaps in our knowledge, we present here results from a study on the effects of three common industrial poly(carboxylic acids) on the formation kinetics and phase morphologies of gypsum. We tested two green inhibitors (PESA and PASP) and two polyacrylic acids with different molecular weights (PAA; as common less-green inhibitors) and derived a mechanistic understanding of the inhibition processes. We document important differences in the crystallization trends in the presence of the different inhibitors, and demonstrate that the additives adsorbed onto the surface of the newly forming gypsum crystals, and changed the shapes and sizes of the resulting crystals. We also demonstrate the significant impact of the molecular weight of polymeric antiscalants on gypsum inhibition efficiencies and illustrate the potential of PESA and PASP as a suitable replacement for the environmentally unfriendly PAA antiscalant to prevent gypsum formation.

## **2. Experimental methods**

Gypsum crystallization solutions were produced by mixing equal volumes of a 200 mM  $\text{CaCl}_2 \cdot 2\text{H}_2\text{O}$  solution (100 % AnalaR Normapour VWR) and a 200 mM  $\text{Na}_2\text{SO}_4$  solution (100 % AnalaR Normapour VWR) in a 1 L reactor at room temperature (21 °C) and under constant and continuous stirring. After Mixing, an additive-free gypsum crystallization solution with a supersaturation index of 0.84 calculated with the geochemical computer code PhreeqC 3.3.3 was obtained<sup>28</sup>.

Polyepoxysuccinic acid sodium salt (40 wt.% in H<sub>2</sub>O) with M<sub>w</sub> ~ 400-1500 Da (PESA<sub><1.5K</sub>), polyaspartic acid sodium salt (40 wt.% in H<sub>2</sub>O) with M<sub>w</sub> ~ 1000-5000 Da (PASP<sub><5K</sub>), provided by Shandong Taihe Water Treatment Technologies Company, and two polyacrylic acids (Sigma-Aldrich) with M<sub>w</sub> ~ 2000 Da (PAA<sub>2K</sub>; 63 wt.% in H<sub>2</sub>O) and ~ 100000 Da (PAA<sub>100K</sub>; 35 wt.% in H<sub>2</sub>O) were added to the initial sodium sulfate solution at a concentration of 40 ppm. This was done prior to mixing of this stock solution with the calcium chloride stock solution. Therefore, once mixed the solutions contained 100 mM Ca<sup>2+</sup>, 100 mM SO<sub>4</sub><sup>2-</sup> and 20 ppm additive. In all experiments, the pH of the mixed solutions was adjusted to ~ 4 or ~ 7, with NaOH and / or HCl.

Changes in the mixed solutions were monitored by measuring the increase in absorbance using a UV-Vis spectrophotometer (Uvikon XL) at  $\lambda = 520$  nm with the angle between the incident beam and detector of 180°. The reactions were followed at room temperature for up to 300 minutes by measuring the absorbance of 3 mL aliquots taken from the mixed solutions. Each experimental set was carried out in triplicate. The absorbance data is plotted as the normalized change in solution turbidity over time.

At the end of each experiment, the solutions were quench-filtered (0.2  $\mu$ m) under vacuum and the solids retrieved. In all experiments, regardless if additives were present or not, the solid end-products were always gypsum as determined by powder X-ray diffraction (XRD; Bruker D8 diffractometer; CuK $\alpha$ 1; 2 $\theta$  range 5 - 35°; resolution 0.105° / step; counting time 1 s / step) with XRD patterns analyzed with the EVA software (version 3) and the PDF-2-1996 database. The morphology of the formed gypsum crystals was imaged using a field emission gun scanning electron microscope (FEG-SEM, FEI Quanta 650, 5 kV). The sizes and shapes of the resulting crystals were evaluated using the ImageJ v. 1.49 software.<sup>29</sup>

Finally, to determine the nature of the surface interactions between the inhibitors and the gypsum end-products, we employed X-ray photoelectron spectroscopy (XPS) with a

detection limit of 0.1 at. % (which is roughly 1ppth or  $10^{19}$  atoms/cm<sup>3</sup>). XPS spectra were acquired from the top 8-10 nm of gypsum crystals using a Kratos Axis Ultra-DLD spectrometer with a monochromatic Al K<sub>α</sub> X-ray source (144 W) and analyzer pass energies of 40 eV (high resolution scans). The base pressure during analysis was ca.  $6 \times 10^{-7}$  Pa. All data were referenced to the C (1s) signal at 284.8 eV and quantified using CasaXPS™ (Version 2.3.15) using elemental sensitivity factors supplied by the manufacturer.

### 3. Results

In the additive-free experiments at both pH values tested ( $\sim 4$  or  $\sim 7$ ), the solutions became turbid after  $\sim 30$  seconds (called induction time). Following crystallization induction, it took  $\sim 30$  minutes for the solutions to reach 100 % turbidity (Figure 1, black data points). However, the addition of the inhibitors at pH  $\sim 7$  affected the induction times and the time to reach a maximum turbidity plateau. In the presence of PESA<sub><1.5K</sub>, the induction time increased  $\sim 3$  fold (to  $\sim 90$  seconds) and it took  $\sim 90$  minutes to reach 100 % turbidity (Figure 1, red data points). In contrast, the presence of PAA<sub>100K</sub> actually accelerated the onset of turbidity, with the first turbidity appearing after  $\sim 10$  seconds. However, after this initial onset only a small increase in total turbidity ( $\sim 5$  %) was reached, and subsequently the turbidity remained suppressed up to  $\sim 40$  minutes. Only in a second stage did the turbidity start to increase sharply again reaching 100 % within the following  $\sim 30$  minutes. The slope of the turbidity increase in this stage was similar to the slope of the turbidity development in the additive-free solution (Figure 1, blue data points). In the presence of the lower molecular weight additive, PAA<sub>2K</sub>, a dramatic increase in the induction time ( $\sim 80$  fold, to  $\sim 40$  minutes) was observed and the slope of the turbidity curve also decreased. The turbidity continued to only gradually increase and it only reached  $\sim 20$  % of the maximum possible

turbidity even after 300 minutes (Figure 1, olive data points). However, the most noticeable effect was observed in the presence of  $\text{PASP}_{<5\text{K}}$ , where no change in turbidity were measured even after 300 minutes (Figure 1, lavender data points). The overall order for inhibition effectiveness was therefore  $\text{PESA}_{<1.5\text{K}} < \text{PAA}_{100\text{K}} < \text{PAA}_{2\text{K}} < \text{PASP}_{<5\text{K}}$ .

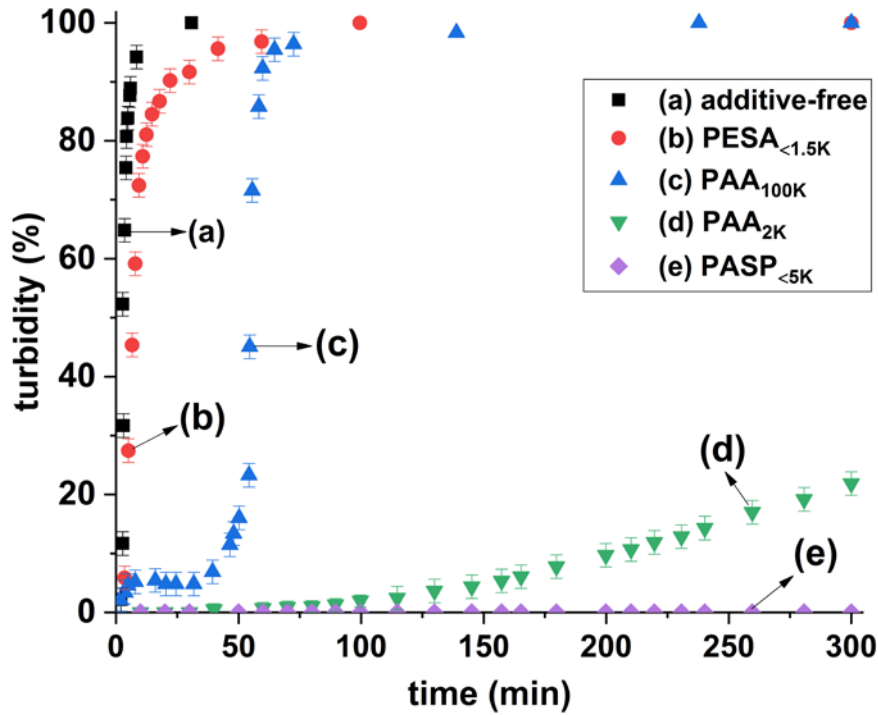


**Figure 1.** The effect of adding 20 ppm  $\text{PESA}_{<1.5\text{K}}$ ,  $\text{PAA}_{100\text{K}}$ ,  $\text{PAA}_{2\text{K}}$  or  $\text{PASP}_{<5\text{K}}$  at  $\text{pH} \sim 7$  on the development of solution turbidity compared to the additive-free gypsum crystallization.

The effects of  $\text{PAA}_{100\text{K}}$  and  $\text{PAA}_{2\text{K}}$  on the onset and the development of turbidity also exhibited a  $\text{pH}$ -dependence (Figure 2). At  $\text{pH} \sim 4$ , with  $\text{PAA}_{100\text{K}}$ , the onset of turbidity was almost the same as that in the additive-free system ( $\sim 30$  seconds). However, the subsequent development of the turbidity was slower and followed a different trend than the additive-free and  $\text{PAA}_{100\text{K}}$  at  $\text{pH} \sim 7$  systems (Figure 2, black vs. blue vs. orange data points). Specifically,



at pH ~ 4 the turbidity remained at a constant ~ 2 % for ~ 50 minutes, and for the next ~ 80 minutes the turbidity only increased slowly and exponentially until reaching ~ 50 %. After this point (~ 130 minutes), the turbidity abruptly increased and reached a plateau within the next ~ 10 minutes (~ 140 minutes after onset) with a slope similar to the slope of the turbidity development in the additive-free system. This clearly documents that PAA<sub>100K</sub> is a more effective inhibitor at pH ~ 4 than ~ 7. On the other hand, for PAA<sub>2K</sub> at pH ~ 4 the first change in turbidity was measured after ~ 25 minutes (in contrary to the induction time of ~ 40 minutes at pH ~ 7) and for the next ~ 210 minutes the turbidity increased exponentially until reaching ~ 60 %. In a final stage, the turbidity then sharply increased and levelled off after ~ 255 minutes with a slope similar to the slope of the turbidity development in the additive-free system (Figure 2, magenta data points). These results indicate that PAA<sub>2K</sub> is a more effective inhibitor at pH ~ 7.

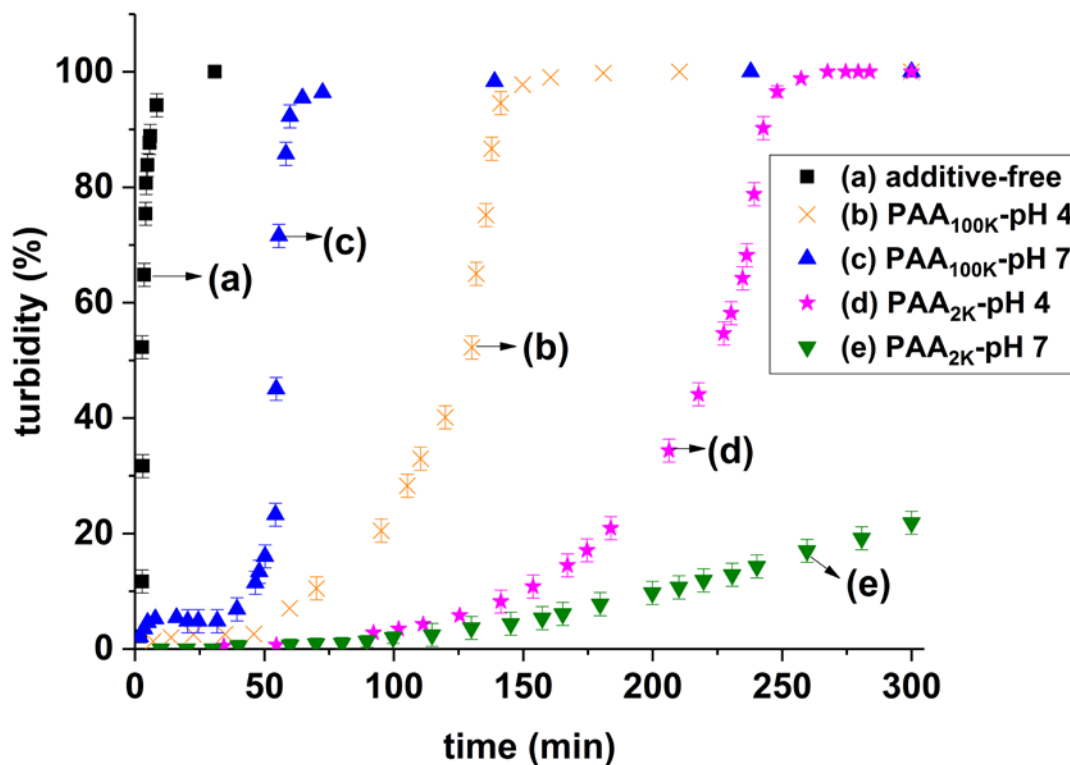


**Figure 2.** The effect of 20 ppm PAA<sub>2K</sub> and PAA<sub>100K</sub> on the development of turbidity at pH ~ 4 and ~ 7. Note that in the additive-free system the turbidity development was equally fast at pH ~ 4 or ~ 7 and thus both are represented by the black squares.

To obtain further insights into the role of the additives in inhibiting gypsum crystallization, the atomic composition of the topmost surface layers of the gypsum crystals precipitated in the absence and presence of the additives were characterized by XPS (Table 1). In this table Ca2p, S2p and O1s represent the atomic percent of these elements in the synthesized gypsum structure. The observed Na1s was due to the presence of Na<sup>+</sup> in the crystallization solution, whilst C1s originates from the adventitious carbon and / or adsorbed carboxylate functional groups related to the tested antiscalants.

**Table 1.** Surface composition of the precipitated gypsum crystals as analyzed by XPS (at. %); note that no gypsum crystals precipitated from solutions containing 20 ppm PASP<sub><5K</sub> at pH ~ 7.

	O 1s	C 1s	Ca 2p	S 2p	Na 1s
Additive-free	58.6	14.7	12.8	13.7	0.2
PESA <sub>&lt;1.5K</sub> -pH ~ 7	61.1	14.9	11.7	12.1	0.2
PAA <sub>2K</sub> -pH ~ 4	53.9	23.8	10.8	11.3	0.2
PAA <sub>2K</sub> -pH ~ 7	52.5	25.7	11.1	10.5	0.2
PAA <sub>100K</sub> -pH ~ 4	57.9	16.6	12.4	12.9	0.2
PAA <sub>100K</sub> -pH ~ 7	58.2	15.1	12.8	13.7	0.2

In addition, the C1s envelope was decomposed into three distinct peaks of C–C, C–O–C and O–C=O groups. Table 2 presents the peak areas of C–C, C–O–C and O–C=O functional groups, which contributed to the total C1s peak area. Besides the absolute peak area values,

the variations in the peak area of O=C=O functional groups adsorbed on gypsum crystals with respect to the changes in the peak area of C-C, were also expressed as O=C=O / C-C peak area ratios ( $R_{(O-C=O / C-C)}$ ). As an example, the C1s XPS spectra for the additive-free and PAA<sub>2K</sub> adsorbed gypsum crystals produced at pH ~ 7 are shown in Figure 3. The results in this figure reveal that in the additive-free sample two main functional groups C-C at 284.7 eV and C-O-C at 286.3 eV, with only a trace amount of O=C=O at 288.93 eV, are present. In contrast, in the PAA<sub>2K</sub> amended sample, although the same two functional groups C-C at 284.6 eV and C-O-C at 285.5 eV were observed, we also observed clear O=C=O moieties at 288.3 eV.

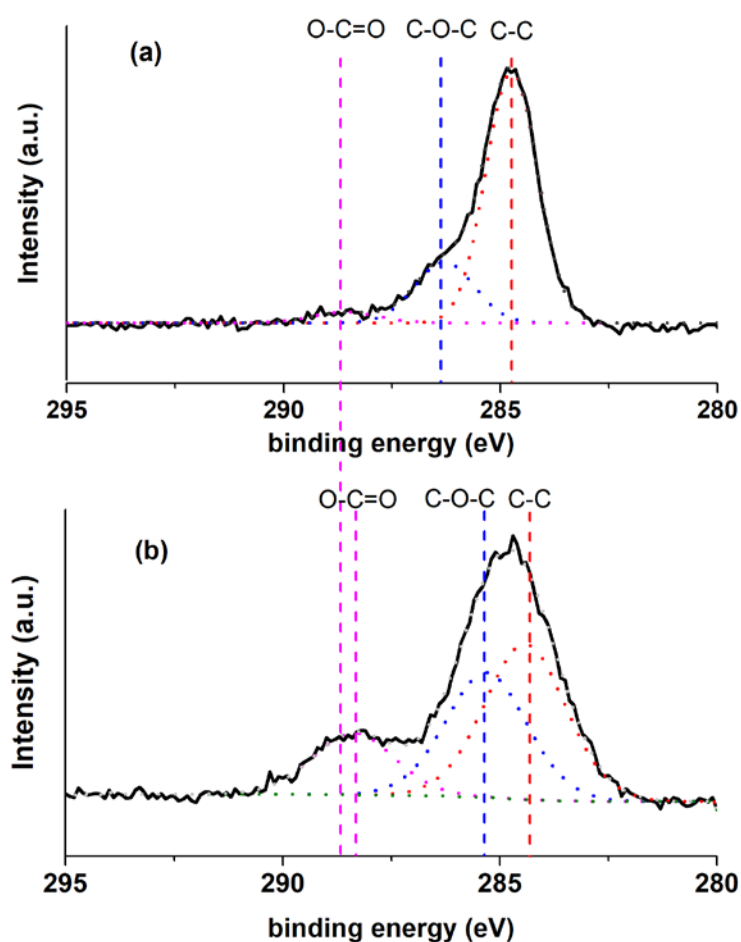


**Figure 3.** XPS spectra of C1s related to the end-product (after 300 min) gypsum crystals from (a) additive-free; (b) 20 ppm PAA<sub>2K</sub> experiments at pH ~ 7; the individual

212 contributions to the fitted envelope of different functional groups are represented with dotted  
213 lines.

214 Table 2. Peak areas of C–C, C–O–C and O–C=O functional groups that contributed to the  
215 total C1s peak area in the XPS spectra on the precipitated gypsum crystals; note that no  
216 gypsum crystals precipitated from solutions containing 20 ppm PASP<sub><5K</sub> at pH ~ 7.

	C-C	C-O-C	O-C=O	R <sub>(O-C=O / C-C)</sub>
Additive-free	79.77	12.16	8.08	0.10
PESA <sub>&lt;1.5K</sub> -pH ~ 7	72.75	18.75	8.51	0.11
PAA <sub>2K</sub> -pH ~ 4	66.48	15.49	18.03	0.27
PAA <sub>2K</sub> -pH ~ 7	45.4	36.47	18.33	0.40
PAA <sub>100K</sub> -pH ~ 4	72.71	13.22	14.07	0.19
PAA <sub>100K</sub> -pH ~ 7	80.9	10.4	8.69	0.13

217

218 It is also worth noting that in Figure 4 the Ca 2p peaks corresponding to calcium ions in the  
219 gypsum structure from the additive-free and PAA<sub>2K</sub> amended experiments appeared at  
220 347.45 eV and 346.65 eV, respectively.

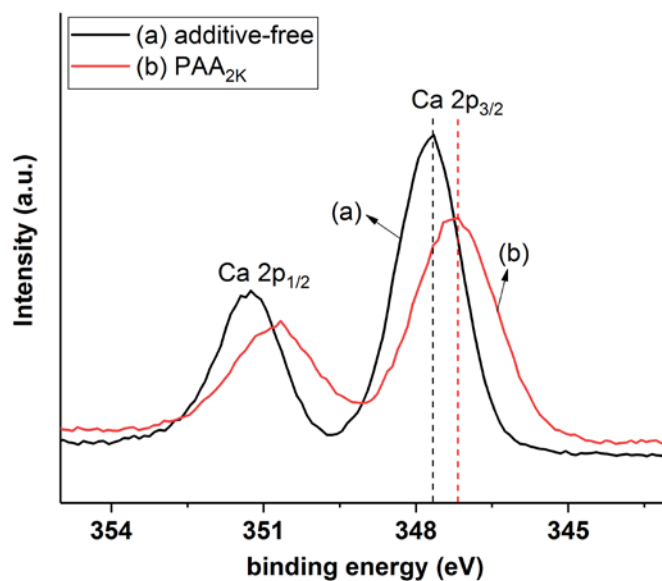


**Figure 4.** XPS spectra of Ca related to the gypsum end-product (after 300 min) from (a) additive-free; (b) 20 ppm PAA<sub>2K</sub> experiments at pH ~ 7.

Morphological changes in the formed gypsum crystals in all experiments were characterized by SEM (Figure 5). The gypsum crystals that formed in the additive-free system and in the presence of 20 ppm PESA<sub><1.5K</sub> and PAA<sub>100K</sub> at pH ~ 7 were mostly large and thin twin crystals (Figure 5 a, b and d). In contrast, adding 20 ppm of PAA<sub>100K</sub> at pH ~ 4 modified the morphology of the gypsum crystals into relatively thick and twinned particles (Figure 5 c). The most profound effect on gypsum morphology and size was observed when PAA<sub>2K</sub> was used as an inhibitor. At pH ~ 4, small irregular gypsum crystals together with some blocky particles of sizes ranging between 2-10  $\mu\text{m}$  were precipitated (Figure 5 e), and in stark contrast at pH ~ 7, loose, tiny crystals with a size range of 20 nm to 5  $\mu\text{m}$  were observed (Figure 5 f).

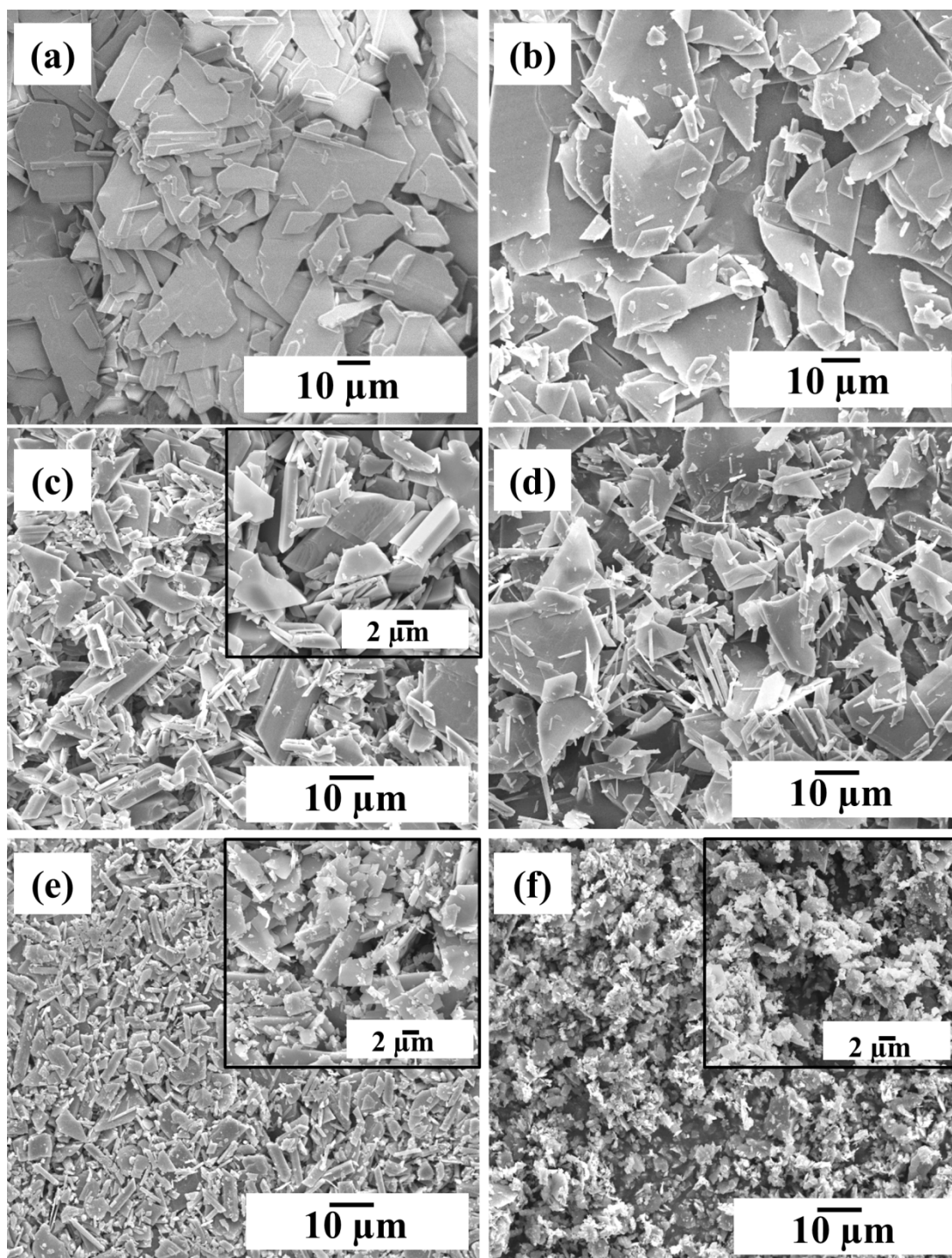


**Figure 5.** SEM micrographs of gypsum crystals collected after 300 minutes in experiments that were (a) additive-free at pH ~ 7; (b) 20 ppm PESA<sub><1.5K</sub> at pH ~ 7; (c) 20 ppm PAA<sub>100K</sub> at pH ~ 4; (d) 20 ppm PAA<sub>100K</sub> at pH ~ 7; (e) 20 ppm PAA<sub>2K</sub> at pH ~ 4; (f) 20 ppm PAA<sub>2K</sub> at pH ~ 7; note that no gypsum crystals precipitated from solutions containing 20 ppm PASP<sub><5K</sub> at pH ~ 7 (see Figure 1).

## 4. Discussion

Measuring turbidity and estimating induction times in the absence and presence of additives is one of the most common methods of evaluating the efficiency of antiscalants in delaying the nucleation and growth of sparingly soluble scale minerals and classifying them as “nucleating” and / or “growth” inhibitors.<sup>1</sup> Our turbidity measurements (Figure 1) revealed that at equal concentrations of 20 ppm and up to 300 minutes of reaction, among the four polymers tested, PASP<sub><5K</sub> fully inhibited gypsum formation (no turbidity occurred). Thus, PASP<sub><5K</sub> is inherently a better gypsum crystallization inhibitor and can be considered a nucleating inhibitor. Whilst, in the presence of PESA and the two PAA additives, gypsum crystals nucleated and grew with different growth rates which was reflected in the slope of the turbidity graphs. Hence, PESA<sub><1.5K</sub> and PAA are classified as growth inhibitors. However, this classification is not absolute and depends on the concentration of the inhibitors or the experimental conditions (e.g., temperature).

Furthermore, in this study (Figure 1 and 2) we have observed the development of turbidity curves that dramatically differ to those in our previous studies where we used carboxylic acid or inorganic inhibitors as additives.<sup>30,31</sup> The observed change in turbidity development likely stems from the differences in the nature of the additives and the mechanisms by which they affected the gypsum crystallization process. Parameters that can affect these inhibition reactions are naturally linked to the inhibition mechanism (e.g., surface adsorption), the factors governing the effectiveness of the polymeric additives (e.g., type and conformation of active functional groups, the molecular structure, and molecular weight of the polyelectrolytes), and the pH of the reacting solutions.

We have previously shown that pH is a main factor controlling the effectiveness of polycarboxylic additives in inhibiting gypsum crystallization because the speciation of the

carboxylic groups is highly pH dependent.<sup>29</sup> Considering the pK values for the tested additives (PASP<sub><5K</sub>: pK 3.25, 4.25;<sup>32</sup> PESA<sub><1.5K</sub>: pK 4.68, 4.92;<sup>33</sup> PAA: pK 4.9<sup>34</sup>) at higher pH (e.g., ~ 7), a greater number of deprotonated carboxylic groups are available in the solution to inhibit gypsum formation. Although sequestration or chelation of cations by COO<sup>-</sup> functional groups has been suggested elsewhere,<sup>35,36</sup> we assert that due to the very low concentration of the antiscalants tested in this research, the inhibition process mainly occurred through surface adsorption.<sup>37</sup>

Besides deprotonation, the solution pH also affects the conformation of polymeric additives (see schematic illustration in Figure 6). For example, PAA is a weak polyelectrolyte and its structure is pH-responsive and undergoes pH dependent conformational changes. Upon addition of PAA to a crystallization solution, due to extensive intermolecular hydrogen bonding, an acidic solution of polymers with a highly coiled structure is produced. With increasing pH, the carboxylic groups are deprotonated and a high amount of negative charge densities are produced, and the polymer chains become extended as a result of electrostatic repulsion.<sup>38</sup> These extended polymer chains are better able to complex with Ca<sup>2+</sup> in solution or on the crystal surfaces (stronger surface adsorption). In our current study, when PAA<sub>2K</sub> is used, an increase in pH from ~ 4 to ~ 7 led to the extended monomers being uniformly distributed in solution and this dramatically inhibited gypsum formation (Figure 2). Indeed, this feature of PAA has been successfully exploited to disperse nanoparticles (e.g., carbon nanotube) at high pH.<sup>39</sup>

In contrast, for the higher molecular weight compound, PAA<sub>100K</sub>, increasing the pH from ~ 4 to ~ 7 led to a faster gypsum formation reaction and less inhibition (Figure 2). This highlights the role of molecular weight of the polymers (which governs the number and conformation of the carboxylic groups) in determining the effectiveness of the inhibitors as well. We assert that at pH ~ 7, upon mixing the sulfate solution containing PAA<sub>100K</sub> with the



calcium solution, due to very high molecular weight and short distances between the monomers, available  $\text{Ca}^{2+}$  ions cross-linked the extended PAA<sub>100K</sub> polymer chains to each other and built a “net-like” structure which decreased the efficiency of the inhibitor. This made the solution immediately turbid (see ~ 5 % turbidity; blue points in Figure 2) and prevented the polymer adsorbing to the nucleating and growing crystals. As a result, by losing the efficiency of the inhibitor, gypsum crystals could easily nucleate and grow (due to the excess of sulfate and  $\text{Ca}^{2+}$  ions not affected by the forming “net-structure”). However, at pH ~ 4, PAA<sub>100K</sub> was slightly deprotonated and is present as an almost coiled configuration, therefore  $\text{Ca}^{2+}$  ions could partially build a “net-structure” (see ~ 2 % turbidity; orange points in Figure 2) and thus most of the coiled PAA<sub>100K</sub> could adsorb onto the nucleating and growing gypsum crystals. Therefore, PAA<sub>100K</sub> yielded higher inhibitory effect at pH ~ 4 than pH ~ 7. Indeed, the role of  $\text{Ca}^{2+}$  in cross-linking PAA polymers and alginates and forming a net-like structure (hydrogels) has been reported also for calcium carbonates.<sup>40,41</sup>

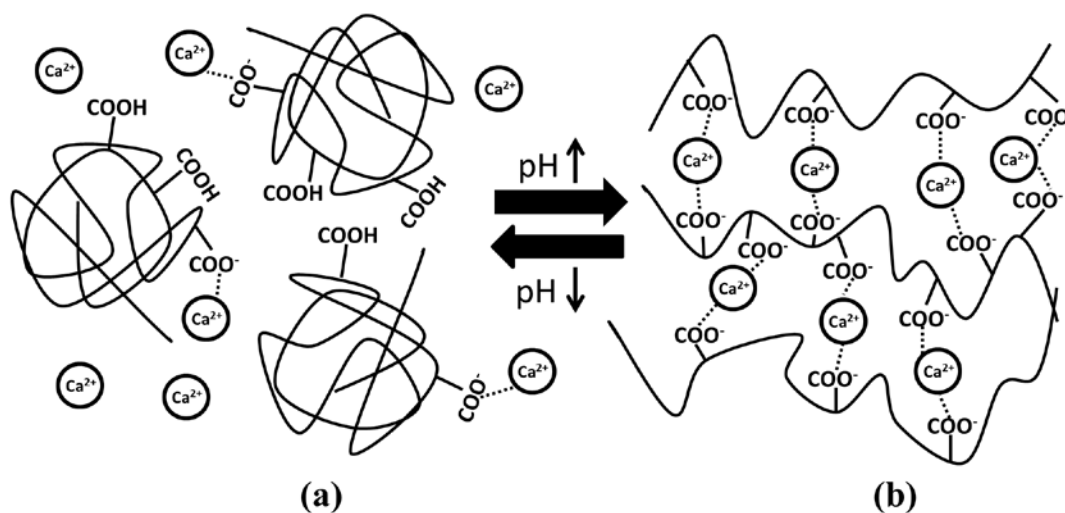


**Figure 6.** Schematic illustration of the effect of pH on the conformation of PAA<sub>100K</sub>; (a) PAA<sub>100K</sub> molecules at pH ~ 4 are only minimally deprotonated and randomly coiled; (b) at pH ~ 7 despite being deprotonated and in their extended conformation, PAA<sub>100K</sub> molecules

form a “net-structure” in the presence of  $\text{Ca}^{2+}$ ; this prevents further  $\text{Ca}^{2+}$  complexation and attachment of the PAA<sub>100K</sub> molecules to the crystal surfaces.

Comparing the efficiency of PAA<sub>100K</sub> with PAA<sub>2K</sub> at constant pH of  $\sim 4$ , reveals the effects that molecular size of a polymeric inhibitor have on its antiscaling efficiency. In this research, PAA<sub>2K</sub> with small molecular chains desorbed too rapidly on gypsum crystals and therefore was more effective, than PAA<sub>100K</sub> which due to longer molecules could not rearrange on the formed crystallite surfaces and wasted most of its mass in trailing ends and loops (Figure 2). In other words, it might become more difficult for PAA<sub>100K</sub> to stretch its polymer chains into an extended configuration<sup>42</sup> which is necessary to adsorb to the crystal surface and thus inhibition of crystallization.<sup>27,43</sup>

It is also worth mentioning that the abrupt increase in turbidity in the presence of PAA<sub>2K</sub> at pH  $\sim 4$  (Figure 2; turbidity of  $\sim 60\%$ ;  $\sim 235$  minutes) and PAA<sub>100K</sub> at pH  $\sim 4$  (Figure 2; turbidity of  $\sim 50\%$ ;  $\sim 130$  minutes) could be attributed to a depletion of the inhibitors from the reacting solution due to surface adsorption during gypsum growth. That means, as the turbidity increased in the mixing solution, nucleation and growth of new particles occurred and the carboxylic functional groups strongly bonded onto the new surfaces and therefore their concentration gradually decreased in solution. This continued until at a certain point where bulk gypsum crystals easily nucleated and grew, as evidenced by the abrupt increase in turbidity with a slope similar to the additive-free system (Figure 2).

This surface adsorption is irreversible because calcium ions in the gypsum structure have a high hydration energy and are highly shielded by structural water molecules and / or the surrounding solution.<sup>44</sup> On the other hand, gypsum has negative surface charge above pH  $\sim 2$  and this implies that surface adsorption of the studied additives should not happen easily.<sup>45</sup> However, taken together these lines of evidence indicate that the carboxylic

functional groups in our used additives did not adsorb onto the gypsum crystals via classical electrostatic interaction (physisorption) but their adsorption occurred through chemisorption. This likely occurred through a “ligand-exchange” mechanism (also known as “specific adsorption” or “coordination adsorption”), during which the carboxylic functional groups replaced the hydroxyl groups linked to the  $\text{Ca}^{2+}$  ions.<sup>46</sup> Similarly, the adsorption of anions onto other hydrated minerals (e.g.,  $\alpha$ -alumina)<sup>47</sup> via ligand-exchange mechanism has been documented.

Considering the mechanisms discussed above,  $\text{PASP}_{<5\text{K}}$  inhibited gypsum formation most effectively due to the presence of high numbers of deprotonated  $\text{COO}^-$  functional groups in the  $\text{PASP}_{<5\text{K}}$  monomer. This enabled  $\text{PASP}_{<5\text{K}}$  to adsorb strongly onto gypsum crystals. In addition, unlike  $\text{PAA}_{100\text{K}}$ , the tested  $\text{PASP}_{<5\text{K}}$  had a molecular weight of  $\sim 1000$ - $5000$  Da, therefore  $\text{Ca}^{2+}$  ions did not cross-link the  $\text{PASP}_{<5\text{K}}$  polymer chains and did not lead to the formation of a “net-like” structure.

Our assertion that surface adsorption plays a major role is supported by our XPS analysis which confirmed the surface adsorption of the additives. The variation in C1s chemical states, especially comparing the  $\text{O}-\text{C}=\text{O}$  binding energy, its peak area, and  $\text{O}-\text{C}=\text{O}$  / C-C peak area ratio (Table 1; Table 2; Figure 3) with the additive-free gypsum crystals helped us to assess the association between the polymers and the surface of gypsum crystals.<sup>48-50</sup> In the absence of additive, the atomic percent of the adventitious carbon contamination<sup>51</sup> was  $\sim 14.7$  at.%. This peak was composed of C-C, C-O-C and  $\text{O}-\text{C}=\text{O}$  groups with peak areas of  $\sim 79.77$  %,  $\sim 12.16$  % and  $\sim 8.08$  %, respectively. The  $R_{(\text{O}-\text{C}=\text{O} / \text{C}-\text{C})}$  in the additive-free system was  $\sim 0.10$ . In the  $\text{PESA}_{<1.5\text{K}}$ -pH  $\sim 7$  system, a minor increase in C1s at.% to  $\sim 14.9$  (with  $\text{O}-\text{C}=\text{O}$  peak area and  $R_{(\text{O}-\text{C}=\text{O} / \text{C}-\text{C})}$  of  $\sim 8.51$  % and  $0.11$ , respectively) was observed indicating a very low adsorption affinity of  $\text{PESA}_{<1.5\text{K}}$  onto the gypsum crystals. This corroborates our turbidity measurements (Figures 1 and 2) and

demonstrates that deprotonated PESA<sub><1.5K</sub>, even at pH ~ 7, was not sufficiently adsorbed onto the gypsum crystals to inhibit the crystallization process. However, in the presence of PAA<sub>2K</sub> at pH ~ 4 and ~ 7, the at.% of C1s increased to ~ 23.8 % and ~ 25.7 % with O–C=O peak area of ~ 18.03 % and ~ 18.33 % and the R<sub>(O–C=O / C–C)</sub> of ~ 0.27 and ~ 0.40, respectively. These data reveal the critical role of increasing pH in deprotonating PAA<sub>2K</sub> carboxylate functional groups and consequently increasing the antiscaling efficiency of this additive by enhancing its adsorption affinity on gypsum crystals (also see Figure 1 and 2). In addition, our XPS analysis revealed that the adsorption of PAA<sub>2K</sub> at ~ 7 was accompanied by a ~ 0.5 eV decrease in O–C=O binding energy, which further confirms the surface adsorption of the polymeric additives by bonding onto the gypsum crystals and is similar to that reported for PAA coated hydroxyapatite powders,<sup>52</sup> and PAA adsorption on alumina.<sup>53</sup>

The data in Tables 1 and 2 reveal that in the PAA<sub>100K</sub> system, the at.% of C1s at pH ~ 4 and ~ 7 was ~ 16.6 % and ~ 15.1 % (with O–C=O peak area of ~ 14.07 % and ~ 8.69 %, R<sub>(O–C=O / C–C)</sub> of ~ 0.19 and ~ 0.13, respectively). It can be seen that both O–C=O peak area and R<sub>(O–C=O / C–C)</sub> at pH ~ 4 and ~ 7 were lower than the corresponding values obtained for the PAA<sub>2K</sub> system. This illustrates the lower adsorption affinity of PAA<sub>100K</sub> on gypsum crystals in comparison to PAA<sub>2K</sub>, which resulted in a fast increase in the turbidity of the crystallization solutions when PAA<sub>100K</sub> was present in the system. In addition, the observed decrease in at.% of C1s and the O–C=O at.% when the pH increased from ~ 4 to ~ 7 was due to the formation of a “net-like” structure at high pH, which decreased the amount of PAA<sub>100K</sub> available to be adsorbed on the gypsum crystals.

Here, it is worth noting that we also documented a ~ 0.6 eV decrease in Ca<sup>2+</sup> binding energy in the PAA<sub>2K</sub> modified gypsum crystals when compared to the additive-free crystals (Figure 4). This observation contradicts previously reported data where an increase in Ca<sup>2+</sup> binding energy of bassanite and gypsum was observed and interpreted as a consequence of

surface adsorption of citric acid <sup>54</sup> and polycarboxylate <sup>55</sup>. Although the reason for this discrepancy in  $\text{Ca}^{2+}$  binding energy is not clear at this stage, it nevertheless documents a change in the chemical environment of  $\text{Ca}^{2+}$  in the formed gypsum crystals because of the surface interactions with the PAA<sub>2K</sub>.

Finally, one striking observation is the effect that the inhibitors had on the morphology and size of the precipitated gypsum crystals (Figure 5). We ascribe this to the surface adsorption of polymers as has previously been demonstrated for other antiscalants with high surface binding.<sup>26</sup> The dominant morphology of the gypsum crystals (irregular, large twins; Figure 5 a) in the additive-free system, was alike to many other previous studies,<sup>56,57</sup> yet it was different to the needle-like morphology that we have reported in our previous additive-free experiments.<sup>30,31</sup> This change in shape could be because of the higher supersaturation (0.84 vs. 0.55) and / or the larger volume of the crystallization solution (1 litre vs. 2 ml) used in the current study,<sup>58</sup> yet a full assessment of these two factors on gypsum formation was outside the scope of this study. In the additive containing solutions, PESA<sub><1.5K</sub> did not cause any morphological changes, which was due to the low carboxyl functional groups and lack of surface adsorption on the fast growing gypsum crystals (Figure 5 b). Interestingly, morphological changes as a result of adsorption of PESA on calcium oxalate have been previously observed <sup>59</sup> but for gypsum this effect was less prominent.

Both PAA<sub>100K</sub> and PAA<sub>2K</sub> when present in solution in a coiled conformation (pH ~ 4) affected the morphology of the resulting crystals. However, because of higher steric hindrance between coils, the larger molecular weight additive exhibited very limited adsorption and this resulted in less surface modification (Figure 5 c) compared to the effects observed at the same condition with PAA<sub>2K</sub> (Figure 5 e). At pH ~ 7, the “net-like-structure” of PAA<sub>100K</sub> decreased the availability of monomers for surface adsorption, and thus the morphologies remained almost similar to those in the additive-free system (Figure 5 d). In

contrast, at pH  $\sim 7$ , highly deprotonated PAA<sub>2K</sub> with a flat configuration was intensely adsorbed and this led to growth inhibition and resultantly small crystals (Figure 5 f). Such tiny crystals are less adhesive to a surface and can therefore be washed away more easily, and thus PAA<sub>2K</sub> is a more effective inhibitor and a more effective crystal modifier for gypsum crystallization than PAA<sub>100K</sub>. Similar gypsum morphology modification in the presence of water soluble polymers (e.g., 5 ppm acrylic acid-allylpolyethoxy maleic carboxylate) have been reported,<sup>60</sup> while the adsorption of PAA on other minerals such as barium sulfate<sup>61</sup> and calcium carbonate<sup>62</sup> have also led to crystal morphology changes.

For the observed morphologies we have schematically illustrated the effects of pH on PAA<sub>2K</sub> conformation and its adsorption in Figure 7.

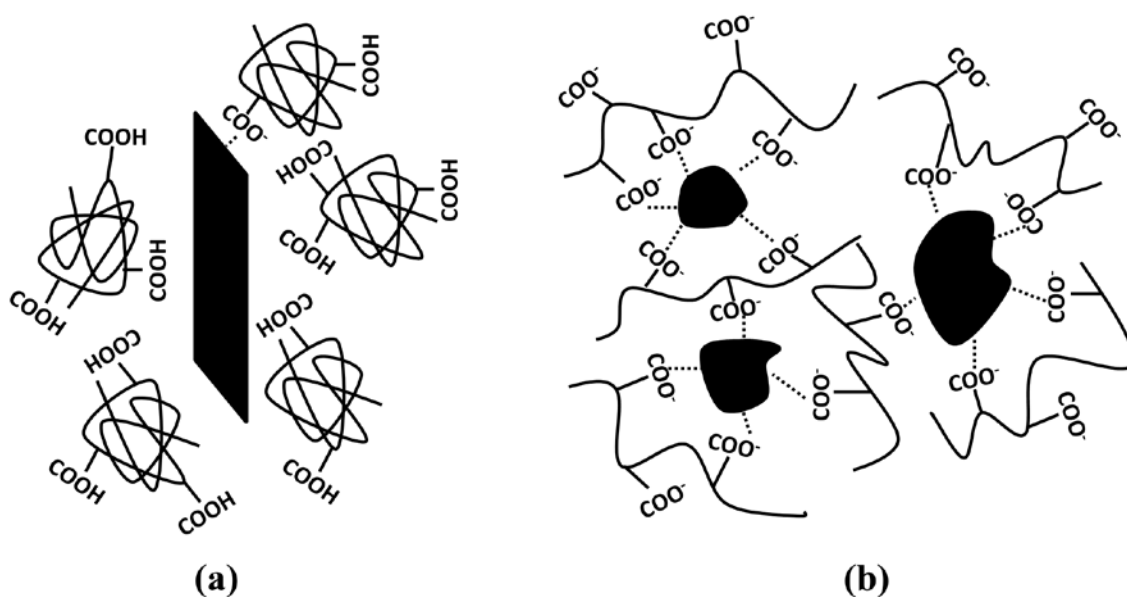


**Figure 7.** A schematic showing the change in gypsum microstructure because of PAA<sub>2K</sub> conformation and its deprotonation; (a) the PAA<sub>2K</sub> molecules are randomly coiled at pH  $\sim 4$  and had limited adsorption on twin or needle like gypsum crystals; (b) deprotonated PAA<sub>2K</sub> molecules are in their extended conformation at pH  $\sim 7$ , deformed the gypsum crystals and prevented growth leading to smaller and more isometric crystals (see also Figure 5 f).

Although we showed that PESA<sub><1.5K</sub> was a less efficient inhibitor, we emphasize that this could probably be due to the higher gypsum supersaturation in this research in comparison to natural fluids where gypsum precipitates (e.g. sea water). However, the potential of both PESA and PASP as promising gypsum antiscalants in industrial plants is well-known,<sup>63</sup> yet we show here what the mechanism is. Furthermore, we also show the potential of green polycarboxylic inhibitors as more effective and efficient additives and suggest that these should replace the non-biodegradable polycarboxylic inhibitors. Our results also revealed the importance of choosing the correct molecular weight antiscalant and the fact that if green inhibitors like PESA and PASP are to be used in an industrial fluid handling system (where gypsum mineral scaling is a problem) they can substantially retard nucleation and growth even at low concentrations. This is not just because they retard nucleation and growth but primarily due to the induced morphological effects. Therefore, the green inhibitors will reduce clogging and surface adhesion to production materials.

## 5. Conclusion

In this study, we documented the effects that polycarboxylic antiscalants have on the nucleation and growth kinetics of gypsum crystals at 21 °C and illustrated the potential of biodegradable PASP and PESA to replace the non-biodegradable PAA additives. 20 ppm of additives affected gypsum formation in the order PESA < PAA < PASP. Our data showed that among the tested additives, PASP completely inhibited gypsum crystallization, while the PAA with low molecular weight, PAA<sub>2K</sub>, increased the induction time and decreased the crystallization kinetics far more than the PAA with the high molecular weight, PAA<sub>100K</sub>. This effect was also pH dependent; with increasing pH from ~ 4 to ~ 7 a positive effect in the efficiency of the PAA<sub>2K</sub> was observed, while for PAA<sub>100K</sub> the opposite was observed, likely

due to the conformational changes in the PAA at near neutral pH. Combining our XPS and turbidity results clearly showed that the depletion of additives in the crystallization solution is a result of their surface adsorption, which in turn caused changes in the morphology of the growing gypsum crystals.

## FUNDING SOURCES

This work was funded by a European Commission Marie Initial Training Research network (Project number 290040) and by the German Helmholtz Recruiting Initiative.

## Acknowledgements

This study was supported by a Marie Curie grant from the European Commission in the framework of the MINSC ITN (Initial Training Research network), Project number 290040 and the German Helmholtz Recruiting Initiative to L.G.B. The authors would like to thank the Cohen Geochemistry Laboratories in the School of Earth and Environment, University of Leeds and the Leeds Electron Microscopy and Spectroscopy Centre (LEMAS) for help and access to instruments during the course of this study.

## References

(1) MacAdam J., Jarvis, P., In *Mineral Scales and Deposits: Scientific and Technological Approaches*, ed. Z. Amjad and K. D. Demadis, Elsevier, Amsterdam, 1<sup>st</sup> ed., 2015, chapter 1, pp 3-47.

(2) Alabi, A.; Chiesa, M.; Garlisi C.; Palmisano, G. Advances in anti-scale magnetic water treatment. *Environ. Sci.: Water Res. & Technol.* **2015**, *1*, 408.

(3) Olajire, A. A. A review of oilfield scale management technology for oil and gas productionm. *J. Petrol. Sci. Eng.* **2015**, *135*, 723.



- (4) Kelland, M.A. Effect of various cations on the formation of calcium carbonate and barium sulfate scale with and without scale inhibitors. *Ind. Eng. Chem. Res.* **2011**, *50*, 5852.
- (5) Demadis, K.D.; Mavredaki, E; Somara, M. Additive-driven dissolution enhancement of colloidal silica. 2. Environmentally friendly additives and natural products. *Ind. Eng. Chem. Res.* **2011**, *50*, 13866.
- (6) Kim, M.M.; Au, J.; Rahardianto, A.; Glater, J.; Cohen, Y.; Gerringer, F.W; Gabelich, C.J. Impact of conventional water treatment coagulants on mineral scaling in RO desalting of brackish water. *Ind. Eng. Chem. Res.* **2009**, *48*, 3126.
- (7) Prisciandaro, M.; Olivieri, E.; Lancia, A; Musmarra, D. Gypsum precipitation from an aqueous solution in the presence of nitrilotrimethylenephosphonic acid. *Ind. Eng. Chem. Res.* **2006**, *45*, 2070.
- (8) Adams, J. F.; Papangelakis, V. G. Gypsum scale formation in continuous neutralization reactors. *Can. Metall. Quart.* **2000**, *39*, 421.
- (9) Rahardianto, A.; Y.Shih, W.; Lee, R. W.; Cohen, Y. Diagnostic characterization of gypsum scale formation and control in RO membrane desalination of brackish water. *J. Membrane Sci.* **2006**, *279*, 655.
- (10) Mi, B.; Elimelech, M. Gypsum scaling and cleaning in forward osmosis: measurements and mechanisms. *Environ. Sci. Technol.* **2010**, *44*, 2022.
- (11) Freyer D.; Voigt, W. Crystallization and phase stability of  $\text{CaSO}_4$  and  $\text{CaSO}_4$ -based salts. *Monatsh. Chem. / Chemi. Monthly* **2003**, *134*, 693.
- (12) Amiri, M.; Moghadasi, J.; Jamialahmadi, M. The Effect of Temperature on Calcium Sulfate Scale Tendency in an Iranian Oil Reservoir and Production Equipment During Water Injection. *Energ Sources Part A* **2013**, *35*, 2264.

- (13) Crabtree, M.; Eslinger, D.; Fletcher, P.; Miller, M.; Johnson A.; King, G. Fighting scale - removal and prevention. *Oilfield Rev.* **1999**, *11*, 30.
- (14) Hasson, D.; Shemer, H.; Sher, A. State of the art of friendly “green” scale control inhibitors: a review article. *Ind. Eng. Chem. Res.* **2011**, *50*, 7601.
- (15) Ketrane, R.; Saidani, B.; Gil, O.; Leleyter L.; Baraud, F. Efficiency of five scale inhibitors on calcium carbonate precipitation from hard water: effect of temperature and concentration. *Desalination* **2009**, *249*, 1397.
- (16) Li, J.; Zhou, Y.; Yao, Q.; Wang, T.; Zhang, A.; Chen, Y.; Wu, W.; Sun, W. Preparation and Evaluation of a Polyether-Based Polycarboxylate as a Kind of Inhibitor for Water Systems. *Ind. Eng. Chem. Res.* **2017**, *56*, 2624.
- (17) Du, K.; Zhou, Y.; Wang, L.; Wang, Y. Fluorescent-tagged no phosphate and nitrogen free calcium phosphate scale inhibitor for cooling water systems. *J. Appl. Polym. Sci.* **2009**, *113*, 1966-1974.
- (18) Zhang, Q.; Zhang, Z.; Teng, J.; Huang, H.; Peng, Q.; Jiao, T.; Hou, L.; Li, B. Highly efficient phosphate sequestration in aqueous solutions using nanomagnesium hydroxide modified polystyrene materials. *Ind. Eng. Chem. Res.* **2015**, *54*, 2940.
- (19) Withers, P. J.; Elser, J. J.; Hilton, J.; Ohtake, H.; Schipper W. J.; Van Dijk, K. C. Greening the global phosphorus cycle: how green chemistry can help achieve planetary P sustainability. *Green Chem.* **2015**, *17*, 2087.
- (20) Belarbi, Z.; Gamby, J.; Makhloufi, L.; Sotta B.; Tribollet, B. Inhibition of calcium carbonate precipitation by aqueous extract of *Paronychia argentea*. *J. Cryst. Growth* **2014**, *386*, 208.
- (21) Jessop, P.; Ahmadpour, F.; Buczynski, M.; Burns, T.; Green Ii, N.; Korwin, R.; Long, D.; Massad, S.; Manley, J.; Omidbakhsh, N. Opportunities for greener alternatives in chemical formulations. *Green Chem.* **2015**, *17*, 2664.

- (22) Liu, D.; Dong, W.; Li, F.; Hui F.; Lédion, J. Comparative performance of polyepoxysuccinic acid and polyaspartic acid on scaling inhibition by static and rapid controlled precipitation methods. *Desalination* **2012**, *304*, 1.
- (23) Gao, Y.; Fan, L.; Ward L.; Liu, Z. Synthesis of polyaspartic acid derivative and evaluation of its corrosion and scale inhibition performance in seawater utilization. *Desalination* **2015**, *365*, 220.
- (24) Prisciandaro, M.; Santucci, A.; Lancia A.; Musmarra, D. Role of citric acid in delaying gypsum precipitation. *Can. J. Chem. Eng.* **2005**, *83*, 586.
- (25) Senthilmurugan, B.; Ghosh, B.; Kundu, S. S.; Haroun M.; Kameshwari, B. Maleic acid based scale inhibitors for calcium sulfate scale inhibition in high temperature application. *J. Petrol. Sci. Eng.* **2010**, *75*, 189.
- (26) Ling, L.; Zhou, Y.; Huang, J.; Yao, Q.; Liu, G.; Zhang, P.; Sun W.; Wu, W. Carboxylate-terminated double-hydrophilic block copolymer as an effective and environmental inhibitor in cooling water systems. *Desalination* **2012**, *304*, 33.
- (27) Amjad Z.; Koutsoukos, P. G. Evaluation of maleic acid based polymers as scale inhibitors and dispersants for industrial water applications. *Desalination* **2014**, *335*, 55.
- (28) Parkhurst, D. L.; Appelo, C. A. J. In U.S. Geological Survey Techniques and Methods; USGS: Reston, VA, 2013; Book 6, Chapter A43, p 497. <http://pubs.usgs.gov/tm/06/a43/>.
- (29) Abràmoff, M. D.; Magalhães P. J.; Ram, S. J. Image Processing with ImageJ. *Biophotonics Inter.* **2004**, *11*, 36.
- (30) Rabizadeh, T.; Peacock C. L.; Benning, L. G. Carboxylic acids: effective inhibitors for calcium sulfate precipitation?. *Mineral. Mag.* **2014**, *78*, 1465.
- (31) Rabizadeh, T.; Stawski, T. M.; Morgan, D. J.; Peacock C. L.; Benning, L. G. The effects of inorganic additives on the nucleation and growth kinetics of calcium sulfate dihydrate crystals. *Cryst. Growth Des.* **2017**, *17*, 582.

- (32) Kokufuta E.; Suzuki, S.; Harada, K. Potentiometric titration behavior of polyaspartic acid prepared by thermal polycondensation. *Biosystems*. **1977**, 9, 211.
- (33) Zhang, L.; Zhu, Z.; Qiu, Y.; Zhang, R.; Zhao, J. Determination of the dissociation constants of polyepoxysuccinic acid. *Front. Env. Sci. Eng.* **2008**, 2, 505.
- (34) De Giglio, E.; Cometa, S.; Cioffi, N.; Torsi, L.; Sabbatini, L. Analytical investigations of poly (acrylic acid) coatings electrodeposited on titanium-based implants: a versatile approach to biocompatibility enhancement. *Anal. Bioanal. Chem.* **2007**, 389, 2055.
- (35) Lioliou, M. G.; Paraskeva, C. A.; Koutsoukos P. G.; Payatakes, A. C. Calcium sulfate precipitation in the presence of water-soluble polymers. *J. Colloid Interf. Sci.* **2006**, 303, 164.
- (36) Sun, X.; Zhang, J.; Yin, C.; Zhang J.; Han, J. Poly (aspartic acid)–tryptophan grafted copolymer and its scale-inhibition performance. *J. Appl. Polym. Sci.* **2015**, 132, 1.
- (37) Wang, H.; Liu, G.; Huang, J.; Zhou, Y.; Yao, Q.; Ma, S.; Cao, K.; Liu, Y.; Wu W.; Sun, W. Performance of an environmentally friendly anti-scalant in CaSO<sub>4</sub> scale inhibition. *Desalination and Water Treatment* **2015**, 53, 8.
- (38) Mountrichas G.; Pispas, S. Synthesis and pH responsive self-assembly of new double hydrophilic block copolymers. *Macromolecules* **2006**, 39, 4767.
- (39) Grunlan, J. C.; Liu L.; Kim, Y. S. Tunable single-walled carbon nanotube microstructure in the liquid and solid states using poly (acrylic acid). *Nano lett.* **2006**, 6, 911.
- (40) Rianasari, I.; Benyettou, F.; Sharma, S. K.; Blanton, T.; Kirmizialtin S.; Jagannathan, R. A Chemical Template for Synthesis of Molecular Sheets of Calcium Carbonate. *Sci. Rep.* **2016**, 6, 2832.

- (41) Wan, L. Q.; Jiang, J.; Arnold, D. E.; Guo, X. E.; Lu H. H.; Mow, V. C. Calcium concentration effects on the mechanical and biochemical properties of chondrocyte-alginate constructs. *Cell. Mol. Bioeng* **2008**, *1*, 93.
- (42) Laguecir, A.; Ulrich, S.; Labille, J.; Fatin-Rouge, N.; Stoll S.; Buffle, J. Size and pH effect on electrical and conformational behavior of poly (acrylic acid): simulation and experiment. *Eur. Polym. J.* **2006**, *42*, 1135.
- (43) Liufu, S.; Xiao H.; Li, Y. Adsorption of poly (acrylic acid) onto the surface of titanium dioxide and the colloidal stability of aqueous suspension. *J. Colloid Interf. Sci.* **2005**, *281*, 155.
- (44) Weijnen M.; Van Rosmalen, G. Adsorption of phosphonates on gypsum crystals. *J. Cryst. Growth* **1986**, *79*, 157.
- (45) Weijnen, M.P.C.; Van Rosmalen G.M.; Van der Leeden, M.C.; In Proc., Intl. Meeting of Geochemistry of Earth Surface and Mineral Formation, ed. R. Rodriguez and Y. Thardy, CSIC-CSIC Press, Madrid, 1<sup>st</sup> ed., 1987, pp. 753.
- (46) Zhang G.; Yu, T., In *Chemistry of Variable Charge Soils*, ed. T. R. Yu, Oxford Univ. Press, New York, 1<sup>st</sup> ed., 1997, chapter 6, pp 175.
- (47) Zorbakhsh, A.; Lee, S.; Welbourn, R.; Clarke, S.; Skoda M.; Clifton, L. Adsorption of sodium hexanoate on  $\alpha$ -alumina. *J. Colloid Interf. Sci.* **2013**, *407*, 348.
- (48) Ni, X.; Liu, Q. The adsorption and configuration of octyl hydroxamic acid on pyrochlore and calcite. *Colloids Surf. A: Physicochem. Eng. Asp.* **2012**, *411*, 80.
- (49) Yoshida, Y.; Van Meerbeek, B.; Nakayama, Y.; Yoshioka, M.; Snauwaert, J.; Abe, Y.; Lambrechts, P.; Vanherle, G; Okazaki, M. Adhesion to and decalcification of hydroxyapatite by carboxylic acids. *J. Dent. Res.* **2001**, *80*, 1565.
- (50) Zhang, S.; Gonsalves, K. E. Influence of the chitosan surface profile on the nucleation and growth of calcium carbonate films. *Langmuir* **1998**, *14*, 6761.

(51) Greczynski G.; Hultman, L. C 1s Peak of Adventitious Carbon Aligns to the Vacuum Level: Dire Consequences for Material's Bonding Assignment by Photoelectron Spectroscopy. *ChemPhysChem*. **2017**, *18*, 1507.

(52) Shen, D.; Fang, L.; Chen X.; Tang, Y. Structure and properties of polyacrylic acid modified hydroxyapatite/liquid crystal polymer composite. *J. Reinf. Plast. Comp.* **2011**, *30*, 1155.

(53) Zhu, H.; Chen, Z.; Sheng Y.; Thi, T. T. L. Flaky polyacrylic acid/aluminium composite particles prepared using in-situ polymerization. *Dyes Pigm.* **2010**, *86*, 155.

(54) Mao, J.; Jiang, G.; Chen Q.; Guan, B. Influences of citric acid on the metastability of  $\alpha$ -calcium sulfate hemihydrate in  $\text{CaCl}_2$  solution. *Colloids Surf. A* **2014**, *443*, 265.

(55) Guan, B.; Ye, Q.; Zhang, J.; Lou W.; Wu, Z. Interaction between  $\alpha$ -calcium sulfate hemihydrate and superplasticizer from the point of adsorption characteristics, hydration and hardening process. *Cement Concrete Res.* **2010**, *40*, 253.

(56) Rubbo, M.; Bruno, M.; Massaro F. R.; Aquilano, D. The five twin laws of gypsum ( $\text{CaSO}_4 \cdot 2\text{H}_2\text{O}$ ): a theoretical comparison of the interfaces of the contact twins. *Cryst. Growth Des.* **2011**, *12*, 264.

(57) Ruiz-Agudo, E.; Álvarez-Lloret, P.; Ibañez-Velasco A.; Ortega-Huertas, M. Crystallographic Control in the Replacement of Calcite by Calcium Sulfates. *Cryst. Growth Des.* **2016**, *16*, 4950.

(58) Rabizadeh, T. The nucleation, growth kinetics and mechanism of sulfate scale minerals in the presence and absence of additives as inhibitors, PhD thesis, University of Leeds, Leeds, December 2016.

- (59) Zhang, Y.; Tang, Y.; Xu, J.; Zhang, D.; Lu G.; Jing, W. Modulation of polyepoxysuccinic acid on crystallization of calcium oxalate. *J. Solid State Chem.* **2015**, *231*, 7.
- (60) Cao, K.; Zhou, Y.; Liu, G.; Wang H.; Sun, W. Preparation and properties of a polyether-based polycarboxylate as an antiscalant for gypsum. *J. Appl. Polym. Sci.* **2014**, *131*, 1.
- (61) Li, J.; Liu, D.; Jiang, H.; Wang, J.; Jing, X.; Chen, R.; Zhu, W.; Han, S.; Li W.; Wei, H. Effects of polyacrylic acid additive on barium sulfate particle morphology. *Mater. Chem. Phys.* **2016**, *175*, 180.
- (62) Ouhenia, S.; Chateigner, D.; Belkhir, M.; Guilmeau E.; Krauss, C. Synthesis of calcium carbonate polymorphs in the presence of polyacrylic acid. *J. Cryst. Growth* **2008**, *310*, 2832.
- (63) Yonghong, S.; Xiang W.; Ying, W. Study on polyepoxysuccinic acid reverse osmosis scale inhibitor. *J. Environ. Sci.* **2009**, *21*, 73.

## Table of Contents Graphic

